ELSEVIER

Physica C 246 (1995) 85–94

PHYSICA C

Spin-fluctuation mediated interaction in the two-dimensional Hubbard model

N. Bulut [a,*,1], D.J. Scalapino [b], S.R. White [c]

[a] Department of Physics, University of Illinois at Urbana-Champaign, Urbana, IL 61801-3080, USA
[b] Department of Physics, University of California, Santa Barbara, CA 93106-9530, USA
[c] Department of Physics, University of California, Irvine, CA 92717-4575, USA

Received 20 February 1995

Abstract

Using Monte Carlo results for the magnetic spin susceptibility and the irreducible electron–electron interaction, we argue that the exchange of para-antiferromagnetic spin fluctuations mediates the effective electron–electron interaction in the doped two-dimensional Hubbard model.

1. Introduction

The nature of the effective interaction between holes in a two-dimensional Hubbard model doped away from half-filling remains a central issue in the problem of understanding the mechanism responsible for pairing in the cuprate superconductors. It is clear that near half-filling the dominant collective excitations in this system are strong short-range nearly antiferromagnetic spin fluctuations. However, it has not been clear whether the effective interaction can be described in terms of the exchange of single longitudinal and transverse spin fluctuations [1,2] or whether higher-order multi-spin-fluctuation processes [3,4] must be taken into account. While a single spin fluctuation exchange interaction has been found to lead to $d_{x^2-y^2}$ pairing [5–7], the question of just how well such a form reproduces the energy and momentum dependence of the effective electron–electron interaction remains open. Here we explore this question by comparing perturbation theory and various diagrammatic forms with results obtained from Monte Carlo simulations.

The calculations which will be described have been done for a two-dimensional Hubbard model with the hamiltonian

$$H = -t \sum_{\langle ij\rangle\sigma} \left(c^{\dagger}_{i\sigma} c_{j\sigma} + c^{\dagger}_{j\sigma} c_{i\sigma} \right) + U \sum_{i} n_{i\uparrow} n_{i\downarrow} . \quad (1)$$

Here $c^{\dagger}_{i\sigma}$ creates an electron of spin σ on site i, t is a one-electron near-neighbor transfer, and U is the on-site Coulomb interaction. The Monte Carlo simulations reported here were carried out for periodic lattices up to 8×8 in size with $U = 4t$ at a filling $\langle n_{i\uparrow} + n_{i\downarrow} \rangle = 0.87$. The lowest temperature considered here is $T = 0.25t$. Thus the momentum resolution on an 8×8 lattice is $\frac{1}{8}$ of the Brillouin zone, and the energy resolution is $\frac{1}{32}$ of the bandwidth. Another estimate of the energy resolution is to note

* Corresponding author.
[1] Present address: Department of Physics, University of California, Santa Barbara, CA 93106-9530, USA.

SSDI 0921-4534(95)00130-1

that if the exchange interaction J is approximated by its strong-coupling form $4t^2/U$, then for $U = 4t$ we have $T = 0.25J$. The basic point is that the results described below provide a description of the interaction on space and time scales which are larger than the characteristic spin-fluctuation correlation length and inverse exchange coupling energy. Thus, even though one is significantly above the temperature at which the interaction may induce pairing correlations, it should be well enough formed to obtain useful insight into its basic structure.

In Section 2, Monte Carlo results for the magnetic susceptibility and the two-particle irreducible vertex, which is the effective interaction, are reviewed. Following this, in Section 3 perturbation theory results through third order are discussed. These provide a feeling for the contribution of various processes. In Section 4 we use skeleton graphs to construct a single spin-fluctuation exchange approximation for the effective interaction and compare this to the Monte Carlo results for the irreducible particle–particle vertex discussed in Section 2. In this calculation we use an approximate particle–hole interaction extracted from the Monte Carlo magnetic susceptibility. In Section 5 we present results in support of this approximation by explicitly calculating the irreducible particle–hole vertex using Monte Carlo simulations and third-order perturbation theory. In the concluding Section 6, we compare a simple phenomenological single spin-fluctuation approximation with the Monte Carlo results. Our conclusion is that for this parameter range, the effective particle–particle interaction can be adequately modeled in terms of the exchange of single longitudinal and transverse spin fluctuations.

2. Monte Carlo results

The structure of the spin fluctuations is reflected in the magnetic spin susceptibility

$$\chi(\boldsymbol{q}, \mathrm{i}\omega_m) = \frac{1}{N}\sum_l \int_0^\beta \mathrm{d}\tau\ \mathrm{e}^{\mathrm{i}(\omega_m\tau - \boldsymbol{q}\cdot\boldsymbol{l})} \times \langle m^-_{i+l}(\tau) m^+_i(0)\rangle. \quad (2)$$

Here $m_i^- = c^\dagger_{i\downarrow} c_{i\uparrow}$, $m_i^-(\tau) = \exp((H-\mu N)\tau) m_i^- \exp(-(H-\mu N)\tau)$, with μ the chemical potential

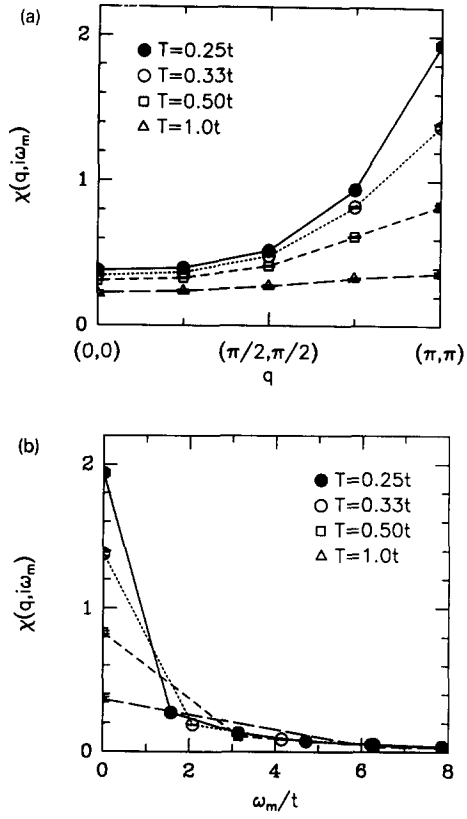

Fig. 1. (a) Momentum dependence of $\chi(\boldsymbol{q}, \mathrm{i}\omega_m = 0)$ along the (1, 1) direction. (b) Matsubara frequency dependence of $\chi(\boldsymbol{q}, \mathrm{i}\omega_m)$ for $\boldsymbol{q} = (\pi, \pi)$. Here results are shown for temperatures $T = 0.25t$ (filled circles), $T = 0.33t$ (open circles), $T = 0.50t$ (open squares) and $T = 1.0t$ (open triangles). χ is given in units where $t = 1$.

and $\omega_m = 2m\pi T$ the usual boson Matsubara frequency. Results for $\chi(\boldsymbol{q}, 0)$ with $\boldsymbol{q}$ varying along the (1, 1) axis are shown in Fig. 1(a) for various temperatures. As the temperature decreases below the exchange energy, the spin susceptibility increases at large values of $\boldsymbol{q}$, indicating the growth of antiferromagnetic correlations. Fig. 1(b) shows the ω_m dependence of $\chi(\boldsymbol{q}, \mathrm{i}\omega_m)$ for $\boldsymbol{q} = (\pi, \pi)$, and one sees the rapid fall-off associated with the spin-fluctuation energy scale. In Fig. 2 we show results for $\chi(\boldsymbol{q}, 0)$ with $T = 0.25t$ on 4×4, 6×6 and 8×8 lattices. This comparison shows that at this temperature, the finite-size effects on the magnetic susceptibility are negligible.

We turn next to the effective particle–particle interaction. Using quantum Monte Carlo simulations,

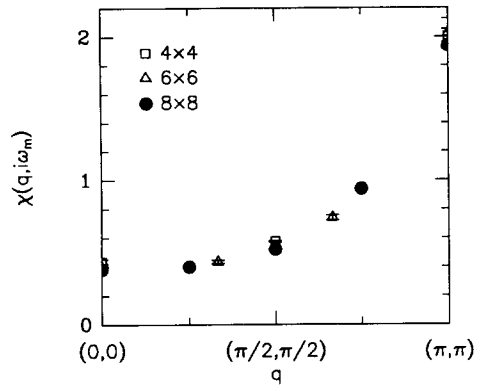

Fig. 2. Momentum dependence of $\chi(\boldsymbol{q}, i\omega_m = 0)$ for different size lattices at $T = 0.25t$.

we have calculated the two-particle Green's function [8]

$$G_2(x_4, x_3, x_2, x_1) = -\langle T c_\uparrow(x_4) c_\downarrow(x_3) c_\downarrow^\dagger(x_2) c_\uparrow^\dagger(x_1)\rangle. \quad (3)$$

Here $c_\sigma^\dagger(x_i)$ with $x_i = (\boldsymbol{l}_i, \tau_i)$ creates an electron of spin σ at site $\boldsymbol{l}_i$ and imaginary time τ_i. T is the usual τ ordering operator. After taking the Fourier transform of both the space and imaginary time variables, this can be expressed as

$$G_2(p', k', k, p) = -\delta_{p,p'}\delta_{k,k'} G_\downarrow(k) G_\uparrow(p) + \frac{T}{N}\delta_{p'+k',p+k} G_\uparrow(p') G_\downarrow(k') \times \Gamma(p', k', k, p) G_\downarrow(k) G_\uparrow(p). \quad (4)$$

Here $p = (\boldsymbol{p}, i\omega_n)$, and $G_\sigma(\boldsymbol{p}, i\omega_n)$ is the Fourier transform of the single-particle Green's function. Thus knowing G_2 and the single-particle Green's function, one can extract the reducible vertex $\Gamma(p', k', k, p)$ from Eq. (4). We are interested in the zero center-of-mass momentum and energy channel, hence we set $k = -p$ and $k' = -p'$. The effective particle–particle interaction is the irreducible particle–particle vertex Γ_I, which is related to Γ through the t matrix equation illustrated in Fig. 3 and given by

$$\Gamma_I(p' \mid p) = \Gamma(p' \mid p) + \frac{T}{N}\sum_k \Gamma(p' \mid k) \times G_\downarrow(-k) G_\uparrow(k) \Gamma_I(k \mid p). \quad (5)$$

Here, $\Gamma(p' \mid p)$ stands for $\Gamma(p', -p', -p, p)$. Then using the Monte Carlo results for Γ and G, we have solved Eq. (5) to find Γ_I.

The effective particle–particle interaction in the singlet channel is given by

$$\Gamma_{Is}(p' \mid p) = \tfrac{1}{2}(\Gamma_I(p' \mid p) + \Gamma_I(-p' \mid p)). \quad (6)$$

In Fig. 4(a), results for Γ_{Is} versus the momentum transfer $\boldsymbol{q} = \boldsymbol{p}' - \boldsymbol{p}$ with $\omega_m = \omega_{n'} - \omega_n = 0$ are plotted for various values of the temperature. Just as for $\chi(\boldsymbol{q}, 0)$, Fig. 1(a), as the temperature is lowered, Γ_{Is} increases at large momenta transfers. The bare interaction U would be just a constant equal to $4t$ on this graph. The Matsubara frequency dependence of Γ_{Is} for $\boldsymbol{q} = (\pi, \pi)$ and $T = 0.25t$ is shown in Fig. 4(b). In order to have an estimate of the finite-size effects on Γ_{Is}, in Fig. 4(c) we show $\Gamma_{Is}(\boldsymbol{q}, i\omega_m = 0)$ versus $\boldsymbol{q}$ obtained on 4×4, 6×6 and 8×8 lattices.

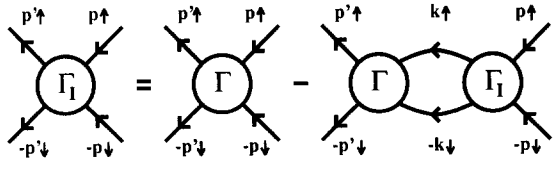

Fig. 3. Feynman diagrams relating the irreducible particle–particle vertex Γ_I to the reducible vertex Γ.

3. Perturbation theory

Fig. 5 shows the diagrams which contribute to Γ_I through third order in U. Here the first-order term U is represented by a single dashed line. The contributions (a) and (h) represent the first two terms in an RPA series corresponding to the exchange of a longitudinal spin fluctuation, while (b) and (e) correspond to the low-order contributions arising from the exchange of a transverse spin fluctuation. Graphs (c) and (d) give negative contributions and following Kanamori [9] can be understood as leading to a reduction [10] in the effective U brought about through particle–particle scattering processes. These multiple scatterings lead to correlations which cause the spin-up and spin-down electrons to avoid each other, reducing the effective U. The leading vertex corrections are shown in graphs (f) and (g).

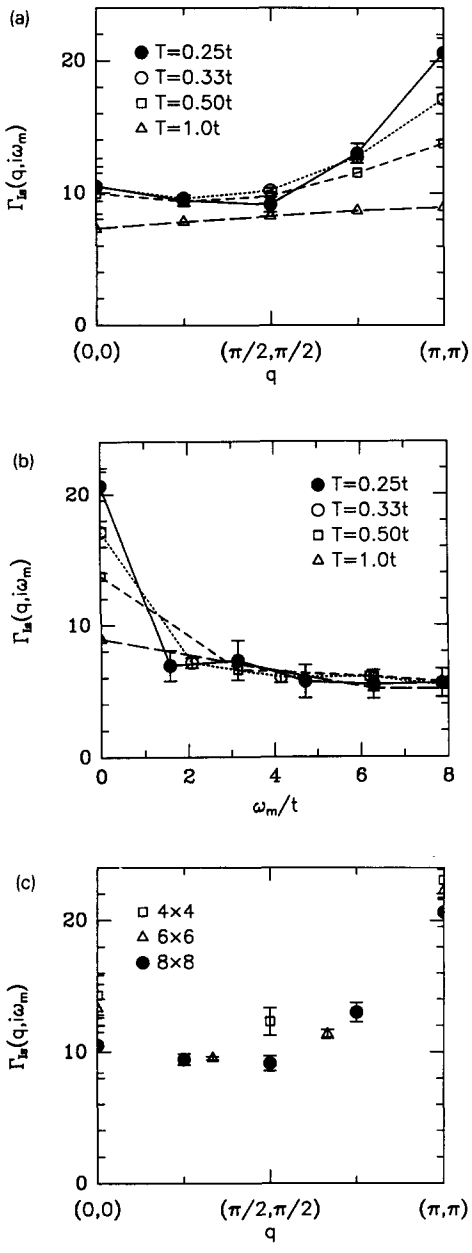

Fig. 4. (a) Momentum dependence of the irreducible vertex in the singlet channel, $\Gamma_{Is}(q, i\omega_m)$, for zero energy transfer $\omega_m = 0$. Here the incoming momentum $p = (\pi, 0)$, the outgoing momentum $p' = p + q$, and $\omega_n = \omega_{n'} = \pi T$. (b) Energy transfer dependence of $\Gamma_{Is}(q, i\omega_m)$ for $q = (\pi, \pi)$, $\omega_n = \pi T$ and $\omega_{n'} = \omega_n + \omega_m$. Here results are given for temperatures $T = 0.25t$ (filled circles), $T = 0.33t$ (open circles), $T = 0.50t$ (open squares), and $T = 1.0t$ (open triangles). (c) Momentum dependence of $\Gamma_{Is}(q, i\omega_m = 0)$ for 4×4, 6×6 and 8×8 lattices at $T = 0.25t$. Γ_{Is} is given in units of t.

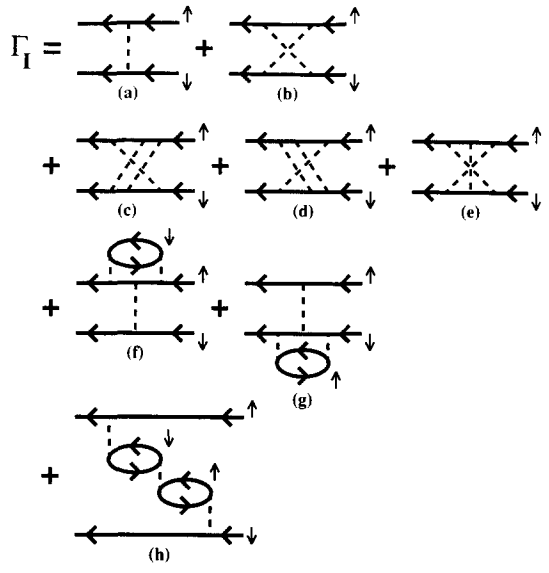

Fig. 5. Feynman diagrams contributing to the irreducible particle–particle interaction through third order in U.

We have evaluated these graphs on an 8×8 lattice with $U = 4t$, and the results of the various contributions are shown versus q for $\omega_m = 0$ in Fig. 6(a) and for $q = (\pi, \pi)$ versus ω_m in Fig. 6(b). The dominant contributions arise from the leading contributions to the spin-fluctuation exchange processes (a), (b), (e), and (h). For $\omega_m = 0$, both the Kanamori renormalization graphs and the vertex corrections act to reduce the strength of the interaction. Their contributions reduce the strength of the $q = (\pi, \pi)$ interaction by about one-third. In Fig. 7, we compare the result obtained by summing the diagrams shown in Fig. 5 with the Monte Carlo result for a temperature $T = 0.25t$. At this temperature, the low-order graphs in Fig. 5 are not adequate to represent the large-momentum behavior of the effective interaction.

4. Single spin-fluctuation exchange approximation

In order to develop a more adequate means for treating the effects of the antiferromagnetic spin fluctuations on the interaction, it is useful to first consider the diagrammatic representation for $\chi(q, i\omega_m)$ shown in Fig. 8. Here χ has been expressed in terms of the dressed single-particle propa-

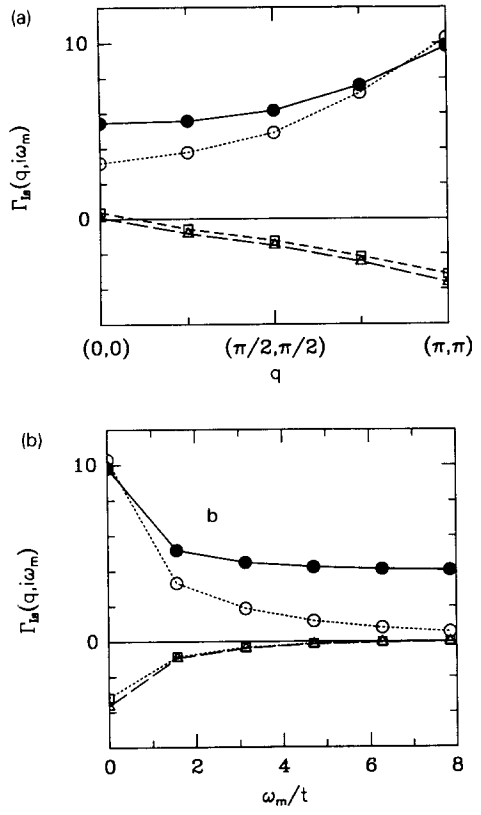

Fig. 6. (a) Momentum and (b) frequency dependence of different classes of diagrams contributing to $\Gamma_{ls}(q, i\omega_m)$ through third order in U. Here the filled circles represent the contribution of the bare U and the longitudinal spin-fluctuation exchange (diagrams of type (a) and (h) in Fig. 5), the open circles represent the contribution of the transverse spin fluctuations (Fig. 5(b) and (e)), the open squares show the ordinary vertex corrections (Fig. 5(f) and (g)), and the open triangles show the Kanamori type of vertex corrections (Fig. 5(c) and (d)). Here $T = 0.25t$.

gator G and the irreducible particle–hole vertex $\bar{\Gamma}_I$. In the following, we will approximate $\bar{\Gamma}_I$ with an effective particle–hole interaction $\bar{U}(q, i\omega_m)$ that depends only on the center-of-mass momentum and frequency, q and ω_m. In Section 5, we will present results in support of this approximation.

With this assumption, the expression for $\chi(q, i\omega_m)$, Fig. 8, simplifies to the RPA form

$$\chi(q, i\omega_m) = \frac{\bar{\chi}(q, i\omega_m)}{1 - \bar{U}(q, i\omega_m)\bar{\chi}(q, i\omega_m)}, \tag{7}$$

with

$$\bar{\chi}(q, i\omega_m) = -\frac{T}{N}\sum_{p, i\omega_n} G(p+q, i\omega_n + i\omega_m)G(p, i\omega_n). \tag{8}$$

Here $G(p, i\omega_n)$ is the dressed single-particle propagator. Monte Carlo results for the momentum dependence of $\bar{\chi}(q, i\omega_m)$ are plotted in Fig. 9(a). Using the Monte Carlo data for $\chi(q, i\omega_m)$ and $\bar{\chi}(q, i\omega_m)$, we obtain $\bar{U}(q, i\omega_m)$ from

$$\bar{U}(q, i\omega_m) = \frac{1}{\bar{\chi}(q, i\omega_m)} - \frac{1}{\chi(q, i\omega_m)}. \tag{9}$$

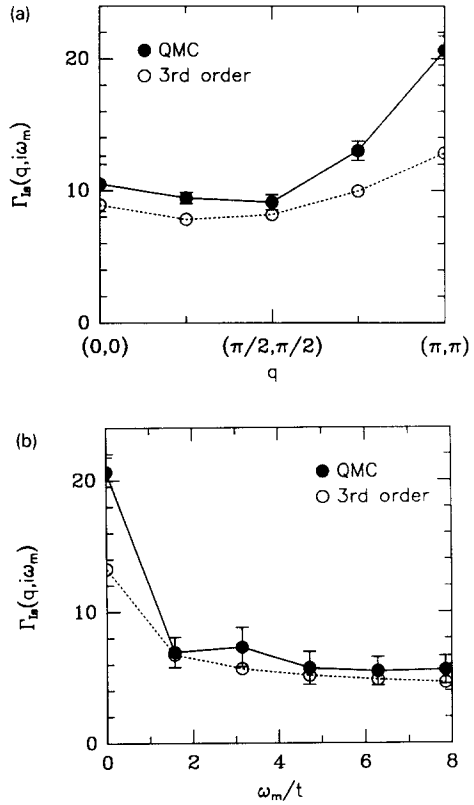

Fig. 7. Comparison of the (a) momentum and (b) frequency dependence of $\Gamma_{ls}(q, i\omega_m)$ obtained from Monte Carlo simulations and the third-order perturbative calculation.

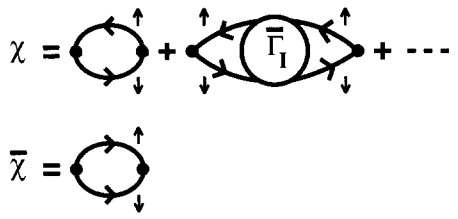

Fig. 8. Diagrammatic representation of the transverse magnetic susceptibility $\chi(\boldsymbol{q}, \mathrm{i}\omega_m)$ in terms of the particle–hole irreducible vertex $\bar{\Gamma}_1$ and the fully dressed single-particle propagator. Here $\bar{\chi}$ is the piece of χ that does not include repeated particle–hole scatterings.

The dependence of $\bar{U}(\boldsymbol{q}, 0)$ on the center-of-mass momentum $\boldsymbol{q}$ is shown in Fig. 9(b). We see that $\bar{U}(\boldsymbol{q}, 0)$ is a smooth function of $\boldsymbol{q}$. At $\boldsymbol{q} = (\pi, \pi)$, $\bar{U}(\boldsymbol{q}, 0)$ is reduced to about 80% from its bare value of $U = 4t$.

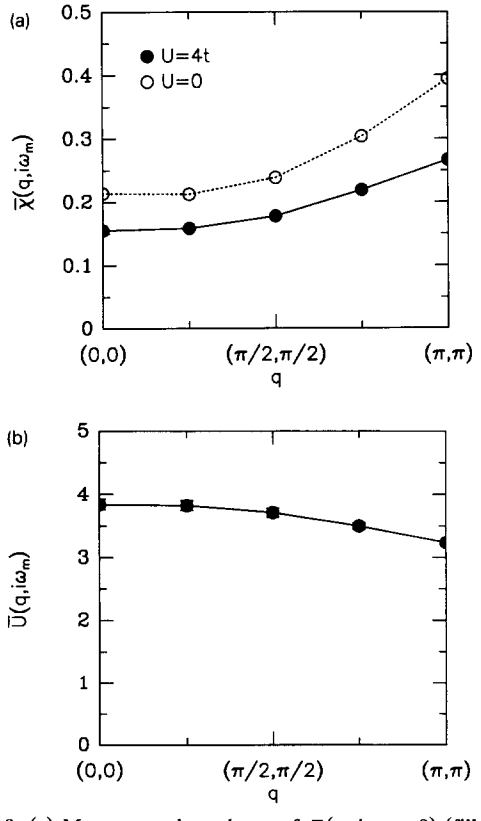

Fig. 9. (a) Momentum dependence of $\bar{\chi}(\boldsymbol{q}, \mathrm{i}\omega_m = 0)$ (filled circles) and the non-interacting susceptibility $\chi_0(\boldsymbol{q}, \mathrm{i}\omega_m = 0)$ (open circles). (b) Center-of-mass momentum dependence of the effective particle–hole irreducible $\bar{U}(\boldsymbol{q}, \mathrm{i}\omega_m = 0)$. Here $T = 0.25t$.

Self-energy effects play a significant role in reducing $\bar{\chi}$ from its non-interacting value χ_0 shown as the open circles in Fig. 9(a). The reduction of $\bar{U}$ from its bare value of $U = 4t$ reflects both the Kanamori [9] repeated particle–particle scattering corrections [10] and vertex corrections.

Turning to the effective electron–electron interaction, in this same spirit, we will replace the dashed lines in Figs. 5(a), (b), (e), and (h) with $\bar{U}(\boldsymbol{q}, \mathrm{i}\omega_m)$ and use dressed Green's functions for the solid lines. Then adding up the infinite series for the single spin-fluctuation exchange, we have

$$\bar{\Gamma}_1(p' \mid p) = \frac{\bar{U}(p'-p)}{1-\bar{U}^2(p'-p)\bar{\chi}^2(p'-p)} + \frac{\bar{U}^2(p'+p)\bar{\chi}(p'+p)}{1-\bar{U}(p'+p)\bar{\chi}(p'+p)}. \quad (10)$$

This has the usual RPA form [11], but here $\bar{\chi}(\boldsymbol{q}, \mathrm{i}\omega_m)$ is given by Eq. (8) which involves the *dressed Green's function*, and $\bar{U}(\boldsymbol{q}, \mathrm{i}\omega_m)$ is the *effective particle–hole interaction* determined from Monte Carlo data on $\chi(\boldsymbol{q}, \mathrm{i}\omega_m)$ and $\bar{\chi}(\boldsymbol{q}, \mathrm{i}\omega_m)$. In this framework there are of course multi-spin-fluctuation vertex corrections and exchange processes [4,12,13] which are neglected. A skeleton graph showing an example of a two-spin-fluctuation exchange process which is not included in Eq. (10) is shown in Fig. 10.

In Figs. 11(a) and (b), the effective singlet interaction

$$\Gamma_{1s}(p' \mid p) = \tfrac{1}{2}(\Gamma_{1s}(p' \mid p) + \Gamma_{1s}(-p' \mid p)) \quad (11)$$

obtained from Eq. (10) is compared with the Monte Carlo results for Γ_{1s}. Both the momentum and fre-

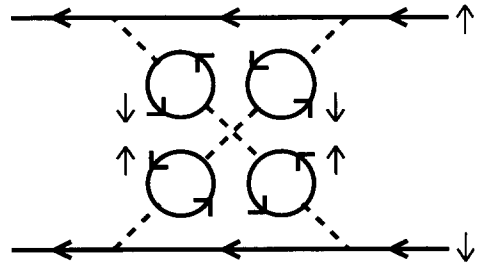

Fig. 10. A skeleton graph contributing to the crossed exchange of spin fluctuations. Diagrams of this type are not included in the RPA calculation of Γ_{1s} given by Eq. (10).

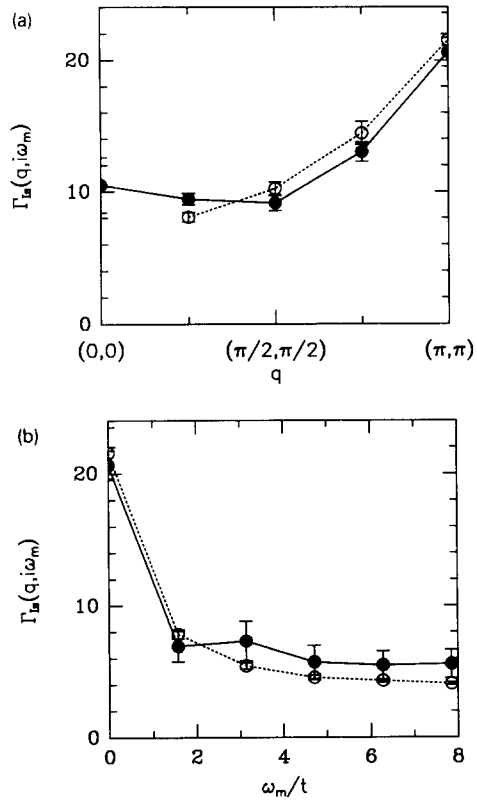

Fig. 11. Comparison of the (a) momentum and (b) frequency dependence of $\Gamma_{Is}(\boldsymbol{q}, i\omega_m)$ obtained from Monte Carlo simulations and the RPA calculation of Eq. (9). Here $T = 0.25t$.

quency dependence are in good agreement with the Monte Carlo results.

5. Irreducible particle–hole vertex $\bar{\Gamma}_I$

In the previous section we presented results for Γ_I obtained from a single spin-fluctuation exchange approximation. In that calculation the irreducible particle–hole vertex was approximated by an effective vertex $\bar{U}$ that depends only on the center-of-mass momentum and energy. In order to justify this assumption, in this section we calculate the irreducible particle–hole vertex $\bar{\Gamma}_I$ using Monte Carlo simulations and third-order perturbation theory. Here we will concentrate on the real part of $\bar{\Gamma}_I$, since it is the dominant part.

The Monte Carlo calculation of $\bar{\Gamma}_I$ is similar to that of the particle–particle vertex Γ_I described in Section 2. We first calculate the two-particle Green's function

$$\bar{G}_2(x_4, x_3, x_2, x_1) = -\langle T c_\uparrow(x_4) c^\dagger_\downarrow(x_3) c_\downarrow(x_2) c^\dagger_\uparrow(x_1)\rangle. \quad (12)$$

In momentum and frequency space, $\bar{G}_2$ can be expressed in terms of the single-particle Green's function $G_\sigma(p)$ and the reducible particle–hole vertex $\bar{\Gamma}$ as

$$\bar{G}_2(p', k', k, p) = \delta_{p,p'}\delta_{k,k'} G_\downarrow(k) G_\uparrow(p) - \frac{T}{N}\delta_{p'-k',p-k} G_\uparrow(p') G_\downarrow(k') \times \bar{\Gamma}(p', k', k, p) G_\downarrow(k) G_\uparrow(p). \quad (13)$$

After extracting $\bar{\Gamma}$ from Eq. (13), we solve the t matrix equation illustrated in Fig. 12. For a given center-of-mass momentum and energy, $Q = (\boldsymbol{Q}, i\omega_{cm})$, the t matrix equation reads

$$\bar{\Gamma}_I(p', p'-Q, p-Q, p) = \bar{\Gamma}(p', p'-Q, p-Q, p) + \frac{T}{N}\sum_k \bar{\Gamma}(p', p'-Q, k-Q, k) \times G_\downarrow(k-Q) G_\uparrow(k) \times \bar{\Gamma}_I(k, k-Q, p-Q, p). \quad (14)$$

The filled circles in Fig. 13(a) and (b) show the real part of $\bar{\Gamma}_I$ for $\boldsymbol{Q} = (\pi, \pi)$ and $\omega_{cm} = 0$ at $T = 0.25t$. Here we denote $\bar{\Gamma}_I(p', p'-Q, p-Q, p)$ by $\bar{\Gamma}_I(\boldsymbol{q}, i\omega_m; \boldsymbol{Q})$, where $\boldsymbol{q} = \boldsymbol{p}' - \boldsymbol{p}$ and $\omega_m = \omega_{n'} - \omega_n$ represent the momentum and energy transfers, respectively. In Fig. 13(a) the results are given for $\omega_n = \omega_{n'} = \pi T$, and in Fig. 13(b) for $\omega_n = \pi T$ and $\omega_{n'} = -\pi T$.

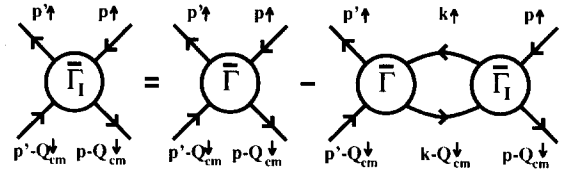

Fig. 12. Particle–hole t matrix equation relating the irreducible vertex $\bar{\Gamma}_I$ to the reducible vertex $\bar{\Gamma}$.

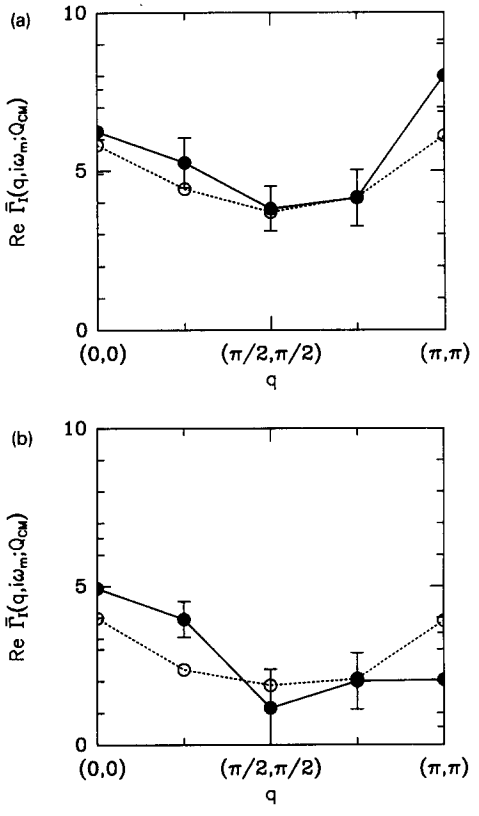

Fig. 13. Momentum dependence of the real part of the irreducible particle–hole vertex $\bar{\Gamma}_I(q, i\omega_m; Q)$ for $Q = (\pi, \pi)$. Here $p = (\pi, 0)$ and $p' = p + q$. The filled circles represent the Monte Carlo data, and the open circles represent the results of the third-order perturbation calculation. In (a) results are given for $\omega_n = \omega_{n'} = \pi T$, and in (b) for $\omega_n = \pi T$ and $\omega_{n'} = -\pi T$. These calculations have been carried out on an 8×8 lattice at $T = 0.25t$.

Next, we calculate $\bar{\Gamma}_I$ within third-order perturbation theory from the Feynman diagrams shown in Fig. 14. These diagrams are very similar to those shown in Fig. 5 for the particle–particle vertex Γ_I, except that here the lower particle lines have been made into hole lines.

Results of the third-order calculation for $\bar{\Gamma}_I(q, i\omega_m; Q)$ are shown by open circles in Figs. 13(a) and (b). We see that the Monte Carlo and the third-order perturbation results for $\bar{\Gamma}_I$ are in good agreement. Both the particle–particle and the particle–hole channels have the longitudinal spin-fluctuation exchange diagrams. However, the transverse spin fluctuations contribute only to the particle–particle irreducible interaction. This is the main cause of

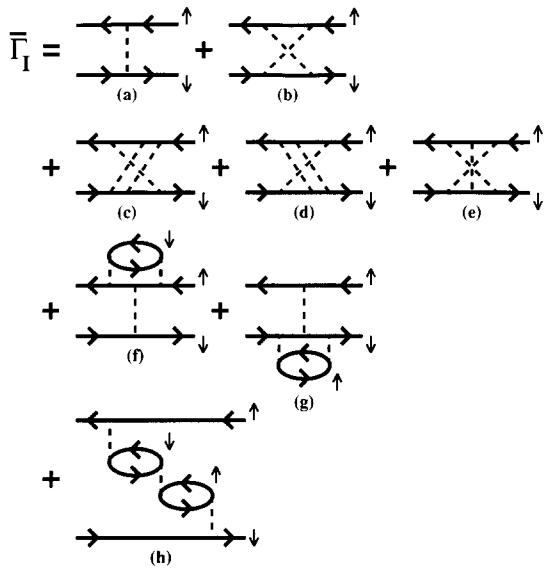

Fig. 14. Feynman diagrams contributing to the particle–hole irreducible vertex $\bar{\Gamma}_I$ through third order in U.

the difference between the third-order perturbation results for $\bar{\Gamma}_I$ shown in Fig. 13 and those for Γ_I shown in Fig. 7(a)

In Section 4 we introduced the effective particle–hole interaction $\bar{U}(Q, i\omega_{cm})$ in order to model $\bar{\Gamma}_I$. In essence, $\bar{U}(Q, i\omega_{cm})$ represents an average $\langle \bar{\Gamma}_I(p', p' - Q, p - Q, p) \rangle_{p,p'}$, where p and p' are on the Fermi surface, and ω_n and $\omega_{n'}$ are

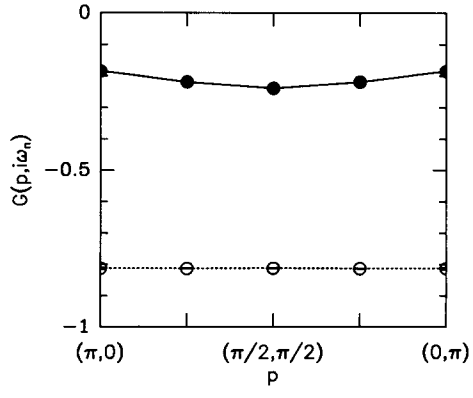

Fig. 15. Real (filled circles) and imaginary (open circles) parts of the single-particle propagator $G(p, i\omega_n)$ vs. p for $\omega_n = \pi T$ at $T = 0.25t$. Here p is varied from $(\pi, 0)$ to $(0, \pi)$ on the Fermi surface of the noninteracting half-filled system.

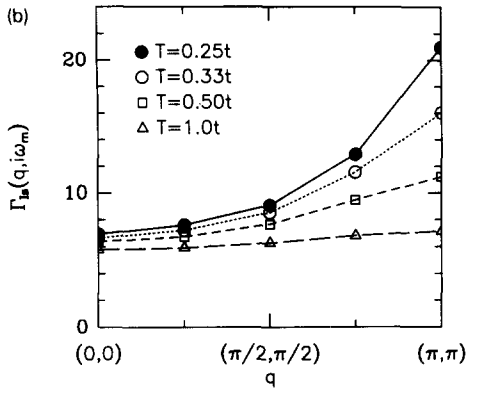

Fig. 16. Momentum dependence of $\Gamma_{Is}(q, i\omega_m)$ obtained from Eq. (15) using $g = 0.8$. Here the results are given at temperatures $T = 0.25t$ (filled circles), $T = 0.33t$ (open circles), $T = 0.50t$ (open squares) and $T = 1.0t$ (open triangles).

restricted to small values. This is a reasonable estimate of $\bar{U}$, especially since the single-particle propagator $G(p, i\omega_n)$ is nearly constant for p on the Fermi surface, as shown in Fig. 15. If we restrict p and p' to the Fermi surface of the half-filled non-interacting system, and also set $|\omega_n| = |\omega_{n'}| = \pi T$, the average value we obtain is $3.6 \pm 0.7t$ at $T = 0.25t$ for $Q = (\pi, \pi)$ and $\omega_{cm} = 0$. This is in reasonable agreement with $\bar{U}(Q = (\pi, \pi), 0) = 3.25t$ shown in Fig. 9(b). These results give support to the simple model that was developed for Γ_I in Section 4.

6. Conclusions

As shown in Section 4, the RPA single spin-fluctuation exchange mediated interaction, when properly renormalized, provides a satisfactory fit to the irreducible particle–particle interaction for the parameter regime we have studied. Here the bare interaction $U = 4t$ corresponds to a weak to intermediate coupling strength in which U is equal to half the bandwidth. One can see, however, that the effective interaction created by U can become quite large, reaching values greater than twice the bandwidth at large momentum transfers. Nevertheless, multi-spin-fluctuation exchange processes as well as spin-fluctuation vertex corrections do not appear to give rise to significant corrections. This is in agreement with calculations of the leading vertex corrections and cross-spin-fluctuation exchange contributions for the two-dimensional Hubbard model [12,13], as well as for a phenomenological spin-fluctuation exchange model [14].

We conclude with a final comparison of Γ_{Is} with a simple phenomenological form,

$$\Gamma_I(q, i\omega_m) = U + \tfrac{3}{2} g^2 U^2 \chi(q, i\omega_m). \quad (15)$$

Here $\chi(q, i\omega_m)$ is the Monte Carlo susceptibility and g is an adjustable dimensionless parameter representing the renormalization of U. At large values of ω_m, $\chi(q, i\omega_m)$ becomes negligible and Γ_I given by Eq. (15) goes to the bare U. Fig. 16 shows Γ_{Is} with $g = 0.8$ versus q for various temperatures. Comparing this with the Monte Carlo Γ_{Is} shown in Fig. 4 shows that the simple approximation of Eq. (15) for Γ_{Is} provides a reasonable fit at large momenta, reproducing the basic features of the effective interaction.

Acknowledgements

We thank N.E. Bickers for helpful discussions. NB would like to acknowledge support by the National Science Foundation (DMR 91-20000) through the Science and Technology Center for Superconductivity, and DJS would like to acknowledge support for this work from the Department of Energy under grant DE-FG03-85ER45197. SRW would like to thank the office of Naval Research for support under grant N00014-91-J-1143. The numerical calculations reported in this paper were performed at the San Diego Supercomputer Center.

References

[1] D.J. Scalapino, E. Loh and J.E. Hirsch, Phys. Rev. B 34 (1986) 8190.
[2] N.E. Bickers, D.J. Scalapino and R.T. Scalettar, Int. J. Mod. Phys. B 1 (1987) 687.
[3] J.R. Schrieffer, X.G. Wen and S.C. Zhang, Phys. Rev. Lett. 60 (1988) 844.
[4] A. Kampf and J.R. Schrieffer, Phys. Rev. B 41 (1990) 6399; ibid. 42 (1990) 7967.
[5] N.E. Bickers, D.J. Scalapino and S.R. White, Phys. Rev. Lett. 62 (1989) 961.

[6] T. Moriya, Y. Takahashi and K. Ueda, J. Phys. Soc. Jpn. 59 (1990) 2905;
idem, Physica C 185–189 (1991) 14.
[7] P. Monthoux and D. Pines, Phys. Rev. Lett. 69 (1992) 961.
[8] N. Bulut, D.J. Scalapino and S.R. White, Phys. Rev. B 47 (1993) 6157.
[9] J. Kanamori, Prog. Theor. Phys. 30 (1963) 275.
[10] L. Chen, C. Bourbonnas, T. Li and A.-M.S. Tremblay, Phys. Rev. Lett. 66 (1991) 369.
[11] N.F. Berk and J.R. Schrieffer, Phys. Rev. Lett. 17 (1966) 433.
[12] K. Yonemitsu, J. Phys. Soc. Jpn. 58 (1989) 4576.
[13] N. Bulut, D.J. Scalapino and S.R. White, Phys. Rev. B 47 (1993) 2742;
N. Bulut and D.J. Scalapino preprint.
[14] A.J. Millis, Phys. Rev. B 45 (1992) 13047.